Enhancing Channel Estimation in RIS-aided Systems via Observation Matrix Design

Zijian Zhang and Mingyao Cui

***Abstract*—Reconfigurable intelligent surfaces (RISs) have emerged as a promising technology for enhancing wireless communications through dense antenna arrays. Accurate channel estimation is critical to unlocking their full performance potential. To enhance RIS channel estimators, this paper proposes a novel observation matrix design scheme. Bayesian optimization framework is adopted to generate observation matrices that maximize the mutual information between received pilot signals and RIS channels. To solve the formulated problem efficiently, we develop an alternating Riemannian manifold optimization (ARMO) algorithm to alternately update the receiver combiners and RIS phase-shift matrices. An adaptive kernel training strategy is further introduced to iteratively refine the channel covariance matrix without requiring additional pilot resources. Simulation results demonstrate that the proposed ARMO-enhanced estimator achieves substantial gains in estimation accuracy over state-of-the-art methods.**

***Index Terms*—Observation matrix design, channel estimation, dense array systems (DAS), densifying MIMO, reconfigurable intelligent surface (RIS).**

I. Introduction

Dense array systems (DASs) integrate massive sub-wavelength antennas within a compact aperture to enhance communication performance. Prominent examples include holographic multi-input multi-output (MIMO) [1], continuous-aperture MIMO [2], super-directive antenna arrays [3], and fluid antenna systems [4]. Recent studies have investigated the impact of practical factors such as phase noise, amplitude errors, and electromagnetic coupling in DASs [5]–[7]. As a representative DAS, reconfigurable intelligent surfaces (RISs) comprise a large number of passive reflecting elements, enabling dynamic manipulation of the wireless environment within a limited aperture. Accurate channel estimation is crucial to support this manipulation [8]. Since RISs typically operate as passive reflectors, channel estimation must recover the high-dimensional transmitter-RIS-receiver cascaded channels. This high dimensionality leads to prohibitive pilot overhead for channel estimation [8].

To reduce this overhead, numerous channel estimation methods have been proposed that exploit inherent channel structures, such as angular-domain sparsity [9], quasi-static channel conditions [10], or common scatterers in multi-user channels [11]. Recently, the learning-based estimator has also been investigated, where an exploration–exploitation strategy is adopted to handle unknown environments [12]. Particularly, to diversify the pilot symbols during channel estimation, existing schemes often employ random phase-shift codebooks [10], [11] or discrete Fourier transform (DFT) codebooks [13] at the receivers and/or RISs to build pilot observation matrices. While feasible, these matrices cannot fully exploit the underlying channel properties of RIS channels, resulting in a suboptimal performance compared to the optimal estimators.

Specifically, as a typical dense array structure, RIS exhibits highly correlated channels due to the closely spaced elements, where the inter-element spacing is often comparable to or smaller than the wavelength. This results in strong spatial correlation among channel coefficients, which has been widely observed in DASs [14], [15]. Exploiting these correlations presents a promising pathway to reduce pilot overhead without compromising estimation accuracy, thereby enhancing existing RIS channel estimators. Such an estimation-enhancing principle has been adopted in other DASs, including densifying MIMO [16] and FASs [17]. For instance, the "ice-filling" technique proposed in [16] demonstrates that aligning the observation matrix with the dominant eigendirections of correlated channels can effectively improve estimation accuracy. In [17], by optimizing the antenna locations for pilot reception, a Bayesian channel estimator is proposed for FASs. However, such methods are designed for point-to-point transceiver links, which are usually not applicable to RIS-aided systems.

To bridge this gap, this paper proposes a novel observation matrix design scheme to enhance channel estimation in RIS-aided systems. The main contributions of this paper are summarized as follows:

- We first formulate a Bayesian observation matrix design framework. It involves the joint design of the RIS phase-shift matrices and the receiver combiners to greedily maximize the mutual information (MI) between the RIS channels and the received pilots.
- To solve the formulated problem efficiently, we develop an alternating Riemannian manifold optimization (ARMO) scheme that alternatively optimizes observation components, which utilizes the information of channel covariance matrix, i.e., kernel.
- Finally, to facilitate kernel acquisition, an adaptive kernel training scheme is proposed to refine the channel estimates and update the kernel iteratively. Simulation results demonstrate that our proposed design can achieve significant gains in estimation accuracy over state-of-the-

This work was supported in part by the National Natural Science Foundation of China under Grant 624B2123.

Zijian Zhang is with the Department of Electronic Engineering, Tsinghua University, Beijing 100084, China, as well as the Beijing National Research Center for Information Science and Technology (BNRist), Beijing 100084, China (e-mail: zhangzij15@tsinghua.org.cn).

Mingyao Cui is with the Department of Electrical and Electronic Engineering, The University of Hong Kong, Hong Kong (e-mail: mycui@eee.hku.hk). *(Corresponding author: Mingyao Cui.)*

art methods.

The remainder of this paper is organized as follows. In Section II, the system model is introduced, and the observation matrix design problem is formulated. In Section III, the proposed ARMO scheme and the kernel training scheme are provided. In Section IV, simulation results are carried out to verify the effectiveness of the proposed schemes. Finally, conclusions are drawn in Section V.

Notation: $[\cdot]^T$, $[\cdot]^H$, $[\cdot]^*$, $[\cdot]^\dagger$, and $[\cdot]^{-1}$ represent the transpose, conjugate-transpose, complex conjugate, pseudo-inverse, and inverse, respectively. The operator $\|\cdot\|$ stands for the l_2-norm. For a matrix $\mathbf{Z}$, $\mathbf{Z}(:,j)$ indicates its j-th column. $\mathrm{Tr}(\cdot)$ specifies the trace, and $\mathrm{diag}(\cdot)$ constructs a diagonal matrix. The expectation operator is given by $\mathsf{E}(\cdot)$, and $\Re(\cdot)$ extracts the real part. A complex Gaussian distribution with mean $\boldsymbol{\mu}$ and covariance matrix $\boldsymbol{\Sigma}$ is written as $\mathcal{CN}(\boldsymbol{\mu}, \boldsymbol{\Sigma})$. $\mathbf{I}_L$ designates the $L \times L$ identity matrix, $\mathbf{1}_L$ an all-ones vector or matrix of dimension L, and $\mathbf{0}_L$ a zero vector of dimension L.

II. System Model and Problem Formulation

In this section, the system model is first introduced in Subsection II-A, Then, the problem of observation matrix design is formulated in Subsection II-B.

A. System Model

This paper considers the uplink channel estimation of an RIS-aided DAS, which is composed of an M-antenna base station (BS) with one radio frequency (RF) chain, an N-element RIS, and a single-antenna user [16]. The antenna spacing of BS and the element spacing of RIS are both on the order of sub-wavelength. The user-RIS channel and the RIS-BS channel are defined as $\mathbf{g} \in \mathbb{C}^N$ and $\mathbf{F}^H \in \mathbb{C}^{M\times N}$, respectively. Let Q denote the number of pilots transmitted by the user in a coherence-time frame. The q-th received pilot at the BS can be modeled as

$$y_q = \mathbf{w}_q^H \mathbf{F}^H \boldsymbol{\Theta}_q \mathbf{g} s_q + n_q, \tag{1}$$

where vector $\mathbf{w}_q \in \mathbb{C}^M$ is the combiner at the BS; diagonal matrix $\boldsymbol{\Theta}_q := \mathrm{diag}(e^{j\theta_1}, \cdots, e^{j\theta_N}) \in \mathbb{C}^{N\times N}$ is the phase shift matrix at the RIS; s_q is the pilot symbol; and $n_q \sim \mathcal{CN}\left(\mathbf{0}, \sigma^2\right)$ is the additive white Gaussian noise (AWGN). Owing to the fully analog architecture, the combiner and phase shift matrix should satisfy the constant-modulus constraints: $|\mathbf{w}_q(m)| = 1/\sqrt{M}$ for all $m \in \{1, \cdots, M\}$ and $|\boldsymbol{\Theta}_q(n,n)| = 1$ for all $n \in \{1, \cdots, N\}$, respectively.

Without loss of generality, we assume that $s_q = 1$ for all $q \in \{1, \cdots, Q\}$. It can be easily proved that, by using some matrix techniques, the original model (1) can be rewritten as

$$y_q = \left(\mathbf{w}_q^H \otimes \boldsymbol{\theta}_q^T\right) \mathbf{h} + n_q = \mathbf{x}_q^H \mathbf{h} + n_q, \tag{2}$$

where $\boldsymbol{\theta}_q := [e^{j\theta_1}, \cdots, e^{j\theta_N}]^T$ is defined as the phase shift vector; $\mathbf{x}_q := \mathbf{w}_q \otimes \boldsymbol{\theta}_q^* \in \mathbb{C}^{MN}$ is the observation vector at timeslot q; and $\mathbf{h}$ is the vectorized equivalent user-RIS-BS channel, defined as

$$\mathbf{h} = \left[\mathbf{g}^H \mathrm{diag}\left(\mathbf{F}\left(:,1\right)\right), \cdots, \mathbf{g}^H \mathrm{diag}\left(\mathbf{F}\left(:,M\right)\right)\right]^H, \tag{3}$$

which is exactly the cascaded channel to be estimated for subsequent beamforming design. Since Q timeslots are utilized for channel estimation, the overall received pilots can be expressed as

$$\mathbf{y} = \mathbf{X}^H \mathbf{h} + \mathbf{n}, \tag{4}$$

where $\mathbf{y} := [y_1^T, \cdots, y_Q^T]^T$, $\mathbf{n} := [\mathbf{n}_1^T, \cdots, \mathbf{n}_Q^T]^T$, and $\mathbf{X} = [\mathbf{x}_1, \cdots, \mathbf{x}_Q]$. This work aims to jointly design combiners $\{\mathbf{w}_q\}_{q=1}^Q$ and precoders $\{\boldsymbol{\theta}_q\}_{q=1}^Q$ so as to better recover channel $\mathbf{h}$ from the received pilots $\mathbf{y}$.

B. Problem Formulation

Since the antenna spacing of the BS and the element spacing of the RIS are small, the cascaded user-RIS-BS channel is strongly correlated due to the high spatial correlations and the electromagnetic mutual coupling among antennas and elements. Let $\boldsymbol{\Sigma}_\mathbf{g} := \mathsf{E}(\mathbf{g}\mathbf{g}^H) \in \mathbb{C}^{N\times N}$ denote the covariance of channel $\mathbf{g}$ and $\boldsymbol{\Sigma}_\mathbf{F} := \mathsf{E}(\mathrm{vec}(\mathbf{F})\mathrm{vec}(\mathbf{F})^H) \in \mathbb{C}^{MN\times MN}$ denote the covariance of channel $\mathbf{F}$, respectively. Assuming the mean of $\mathbf{h}$ is zero, the covariance of the equivalent channel $\mathbf{h}$ can be derived from (3) as $\boldsymbol{\Sigma}_\mathbf{h} := \mathsf{E}\left(\mathbf{h}\mathbf{h}^H\right) = \boldsymbol{\Sigma}_\mathbf{F}^* \odot \left(\mathbf{1}_{M,M} \otimes \boldsymbol{\Sigma}_\mathbf{g}\right)$, which is known as the *kernel* of channel. The high spatial correlation and the mutual coupling indicate that the kernel $\boldsymbol{\Sigma}_\mathbf{h}$ is structured and underdetermined, which can provide prior knowledge for achieving high-accuracy channel estimation [18], [19]. To realize this potential, we adopt the idea of Gaussian process regression (GPR) to design the observation matrix $\mathbf{X}$. Specifically, the channel is modeled as being sampled from the Gaussian process $\mathcal{CN}\left(\mathbf{0}_{MN}, \boldsymbol{\Sigma}_\mathbf{h}\right)$. The joint probability distribution of $\mathbf{h}$ and $\mathbf{y}$ then satisfies

$$\begin{bmatrix} \mathbf{h} \\ \mathbf{y} \end{bmatrix} \sim \mathcal{CN}\left(\begin{bmatrix} \mathbf{0}_{MN} \\ \mathbf{0}_Q \end{bmatrix}, \begin{bmatrix} \boldsymbol{\Sigma}_\mathbf{h} & \boldsymbol{\Sigma}_\mathbf{h}\mathbf{X} \\ \mathbf{X}^H\boldsymbol{\Sigma}_\mathbf{h} & \mathbf{X}^H\boldsymbol{\Sigma}_\mathbf{h}\mathbf{X} + \sigma^2\mathbf{I}_Q \end{bmatrix}\right). \tag{5}$$

Thereby, the posterior mean and the posterior covariance of $\mathbf{h}$ are expressed as

$$\hat{\mathbf{h}} := \boldsymbol{\mu}_{\mathbf{h}|\mathbf{y}} = \boldsymbol{\Sigma}_\mathbf{h}\mathbf{X}\left(\mathbf{X}^H\boldsymbol{\Sigma}_\mathbf{h}\mathbf{X} + \sigma^2\mathbf{I}_Q\right)^{-1}\mathbf{y}, \tag{6}$$

$$\boldsymbol{\Sigma}_{\mathbf{h}|\mathbf{y}} = \boldsymbol{\Sigma}_\mathbf{h} - \boldsymbol{\Sigma}_\mathbf{h}\mathbf{X}\left(\mathbf{X}^H\boldsymbol{\Sigma}_\mathbf{h}\mathbf{X} + \sigma^2\mathbf{I}_Q\right)^{-1}\mathbf{X}^H\boldsymbol{\Sigma}_\mathbf{h}, \tag{7}$$

which yield the optimal channel estimator $\hat{\mathbf{h}} := \boldsymbol{\mu}_{\mathbf{h}|\mathbf{y}}$ and the corresponding estimation error $\boldsymbol{\Sigma}_{\mathbf{h}|\mathbf{y}}$.

Notably, the posterior covariance $\boldsymbol{\Sigma}_{\mathbf{h}|\mathbf{y}}$ depends strongly on the observation matrix $\mathbf{X}$. Hence, carefully designed combiners and precoders $\{\mathbf{w}_q\}_{q=1}^Q$ and $\{\boldsymbol{\theta}_q\}_{q=1}^Q$, i.e., $\{\mathbf{x}_q\}_{q=1}^Q$, can significantly reduce the channel estimation error. Motivated by this, GPR aims to generate observation matrices that extract as much information about $\mathbf{h}$ as possible from the received signal $\mathbf{y}$. Following this principle, our objective is to find $\{\mathbf{w}_q\}_{q=1}^Q$ and $\{\boldsymbol{\theta}_q\}_{q=1}^Q$ that maximize the MI between $\mathbf{y}$ and $\mathbf{h}$, which is formulated as

$$\begin{aligned} \max_{\{\mathbf{w}_q\}_{q=1}^Q, \{\boldsymbol{\theta}_q\}_{q=1}^Q} \quad & I(\mathbf{y};\mathbf{h}) = \log_2 \det\left|\mathbf{I}_Q + \frac{1}{\sigma^2}\mathbf{X}^H\boldsymbol{\Sigma}_\mathbf{h}\mathbf{X}\right| \\ \text{s.t.} \quad & |\mathbf{w}_q| = \frac{1}{\sqrt{M}}\mathbf{1}_M, \quad \forall q \in \{1, \cdots, Q\}, \\ & |\boldsymbol{\theta}_q| = \mathbf{1}_N, \quad \forall q \in \{1, \cdots, Q\}, \end{aligned} \tag{8}$$

which resembles a classical water-filling problem in MIMO precoding. Note that, solving this problem faces two challenges. First, the coupled combiners $\{\mathbf{w}_q\}_{q=1}^Q$ and phase-shift vectors $\{\boldsymbol{\theta}_q\}_{q=1}^Q$ in observation matrix leads to a non-convex objective function $I(\mathbf{y};\mathbf{h})$. Second, the constant-modulus constraints make it difficult to adopt conventional numerical algorithms. Besides, at the early stage of algorithmic implementations in practice, the knowledge of kernel $\boldsymbol{\Sigma}_\mathbf{h}$ should be determined.

III. Proposed Observation Matrix Design

To solve the above problem, in this section, we first focus on the joint design of $\{\mathbf{w}_q\}_{q=1}^Q$ and $\{\boldsymbol{\theta}_q\}_{q=1}^Q$ for a given kernel $\boldsymbol{\Sigma}_\mathbf{h}$ in Subsection III-A. Then, the acquisition of $\boldsymbol{\Sigma}_\mathbf{h}$ is addressed in Subsection III-B.

A. Observation Matrix Design Using Greedy Method

Due to the above challenges, obtaining the globally optimal solution to problem (8) is intractable. To address this issue, we propose a greedy method that designs $\mathbf{X}$ in a column-by-column manner, i.e., generating $\{\mathbf{w}_q\}_{q=1}^Q$ and $\{\boldsymbol{\theta}_q\}_{q=1}^Q$ sequentially on a pilot-by-pilot basis. Specifically, we define $\mathbf{X}_t = [\mathbf{x}_1, \mathbf{x}_2, \cdots, \mathbf{x}_t]$ as the overall observation matrix for timeslots from 1 to t. Let $\mathbf{y}_t = \mathbf{X}_t^H\mathbf{h} + \mathbf{n}_t$ denote the corresponding received signal, wherein $\mathbf{y}_t = [y_1, y_2, \cdots, y_t]^T$ and $\mathbf{n}_t := [n_1, \cdots, n_t]^T$. Given the current combiners $\{\mathbf{w}_q\}_{q=1}^t$ and phase-shift vectors $\{\boldsymbol{\theta}_q\}_{q=1}^t$ in the first t timeslots, our greedy strategy aims to find the combiner $\mathbf{w}_{t+1}$ and the phase-shift matrix $\boldsymbol{\theta}_{t+1}$ in the next timeslot, such that the MI increment $\Delta I_{t+1} := I(\mathbf{y}_{t+1};\mathbf{h}) - I(\mathbf{y}_t;\mathbf{h})$ from timeslot t to $t+1$ is maximized. In specific, the MI increment ΔI_{t+1} can be calculated from:

$$\begin{aligned} I(\mathbf{y}_{t+1};\mathbf{h}) &= \log_2\det\left|\mathbf{I}_{t+1} + \frac{1}{\sigma^2}\mathbf{X}_{t+1}^H\boldsymbol{\Sigma}_\mathbf{h}\mathbf{X}_{t+1}\right| \\ &= \log_2\det\left|\begin{array}{cc} \mathbf{I}_t + \frac{1}{\sigma^2}\mathbf{X}_t^H\boldsymbol{\Sigma}_\mathbf{h}\mathbf{X}_t & \frac{1}{\sigma^2}\mathbf{X}_t^H\boldsymbol{\Sigma}_\mathbf{h}\mathbf{x}_{t+1} \\ \frac{1}{\sigma^2}\mathbf{x}_{t+1}^H\boldsymbol{\Sigma}_\mathbf{h}\mathbf{X}_t & 1 + \frac{1}{\sigma^2}\mathbf{x}_{t+1}^H\boldsymbol{\Sigma}_\mathbf{h}\mathbf{x}_{t+1} \end{array}\right| \\ &= \log_2\det\left|\begin{array}{cc} \mathbf{I}_t + \frac{1}{\sigma^2}\mathbf{X}_t^H\boldsymbol{\Sigma}_\mathbf{h}\mathbf{X}_t & \frac{1}{\sigma^2}\mathbf{X}_t^H\boldsymbol{\Sigma}_\mathbf{h}\mathbf{x}_{t+1} \\ \mathbf{0} & 1 + \frac{1}{\sigma^2}\mathbf{x}_{t+1}^H\boldsymbol{\Sigma}_t\mathbf{x}_{t+1} \end{array}\right| \\ &= I(\mathbf{y}_t;\mathbf{h}) + \log_2\left(1 + \frac{1}{\sigma^2}\mathbf{x}_{t+1}^H\boldsymbol{\Sigma}_t\mathbf{x}_{t+1}\right). \end{aligned} \tag{9}$$

Thus, the $(t+1)$-th subproblem can be formulated as

$$\begin{aligned} \max_{\mathbf{w}_{t+1},\boldsymbol{\theta}_{t+1}} \quad & \Delta I_{t+1} = \log_2\left(1 + \mathbf{x}_{t+1}^H\boldsymbol{\Sigma}_t\mathbf{x}_{t+1}\right) \\ \text{s.t.} \quad & |\mathbf{w}_{t+1}| = \frac{1}{\sqrt{M}}\mathbf{1}_M,\ |\boldsymbol{\theta}_{t+1}| = \mathbf{1}_N, \end{aligned} \tag{10}$$

where $\mathbf{x}_{t+1} := \mathbf{w}_{t+1} \otimes \boldsymbol{\theta}_{t+1}^* \in \mathbb{C}^{MN}$ is the observation vector at timeslot q. In particular, $\boldsymbol{\Sigma}_t$ is the posterior kernel of channel $\mathbf{h}$, which can be updated by

$$\begin{aligned} \boldsymbol{\Sigma}_t &= \boldsymbol{\Sigma}_\mathbf{h} - \boldsymbol{\Sigma}_\mathbf{h}\mathbf{X}_t\left(\mathbf{X}_t^H\boldsymbol{\Sigma}_\mathbf{h}\mathbf{X}_t + \sigma^2\mathbf{I}_t\right)^{-1}\mathbf{X}_t^H\boldsymbol{\Sigma}_\mathbf{h} \\ &\overset{(a)}{=} \boldsymbol{\Sigma}_{t-1} - \frac{\boldsymbol{\Sigma}_{t-1}\mathbf{x}_t\mathbf{x}_t^H\boldsymbol{\Sigma}_{t-1}}{\mathbf{x}_t^H\boldsymbol{\Sigma}_{t-1}\mathbf{x}_t + \sigma^2}, \end{aligned} \tag{11}$$

where (a) holds according to [16, Appendix A]. However, due to the coupled combiner $\mathbf{w}_{t+1}$ and the phase-shift vector $\boldsymbol{\theta}_{t+1}$ as well as the constant-modulus constraint, finding the optimal solution to problem (10) is challenging. As a suboptimal strategy, an ARMO scheme is proposed to jointly design $\mathbf{w}_{t+1}$ and $\boldsymbol{\theta}_{t+1}$, which is summarized in **Algorithm 1**. The algorithmic details are explained as follows.

Algorithm 1 ARMO scheme for observation matrix design

Input: Number of pilots Q, kernel $\boldsymbol{\Sigma}_\mathbf{h}$.

Initialize $\boldsymbol{\Sigma}_0 = \boldsymbol{\Sigma}_\mathbf{h}$
for $t = 0, \cdots, Q-1$ **do**
  Randomly generate $\mathbf{w}_{t+1}$ and $\boldsymbol{\theta}_{t+1}$
  while No convergence of MI increment ΔI_{t+1} **do**
    Update iteration parameters: $K \leftarrow M$, $\mathbf{U} \leftarrow (\mathbf{I}_M \otimes \boldsymbol{\theta}_{t+1}^T)\boldsymbol{\Sigma}_t(\mathbf{I}_M \otimes \boldsymbol{\theta}_{t+1}^*)$, $\rho \leftarrow 1/\sqrt{M}$, $\alpha \leftarrow K\lambda_{\max}(\mathbf{U})/4$, $\beta \leftarrow 1/(\lambda_{\max}(\mathbf{U}) + 2\alpha)$
    while No convergence of $f(\mathbf{w}_{t+1})$ **do**
      Update Euclidean gradient $\nabla f(\mathbf{w}_{t+1})$ via (17)
      Update Riemannian gradient $\mathbf{d}_S(\mathbf{w}_{t+1})$ via (18)
      $\mathbf{w}_{t+1} \leftarrow \exp\left(j\angle\left(\mathbf{w}_{t+1} + \beta\mathbf{d}_S(\mathbf{w}_{t+1})\right)\right)/\sqrt{M}$
    end while
    Update iteration parameters: $K \leftarrow N$, $\mathbf{U} \leftarrow \sum_{m=1}^M\sum_{m'=1}^M w_{t+1,m}w_{t+1,m'}^*\boldsymbol{\Sigma}_{t,m,m'}^*$, $\rho \leftarrow 1$, $\alpha \leftarrow K\lambda_{\max}(\mathbf{U})/4$, $\beta \leftarrow 1/(\lambda_{\max}(\mathbf{U}) + 2\alpha)$
    while No convergence of $f(\boldsymbol{\theta}_{t+1})$ **do**
      Update Euclidean gradient $\nabla f(\boldsymbol{\theta}_{t+1})$ via (17)
      Update Riemannian gradient $\mathbf{d}_S(\boldsymbol{\theta}_{t+1})$ via (18)
      $\boldsymbol{\theta}_{t+1} \leftarrow \exp\left(j\angle\left(\boldsymbol{\theta}_{t+1} + \beta\mathbf{d}_S(\boldsymbol{\theta}_{t+1})\right)\right)$
    end while
  end while
  Calculate observation vector: $\mathbf{x}_{t+1} = \mathbf{w}_{t+1} \otimes \boldsymbol{\theta}_{t+1}^*$
  Calculate kernel: $\boldsymbol{\Sigma}_{t+1} = \boldsymbol{\Sigma}_t - \frac{\boldsymbol{\Sigma}_t\mathbf{x}_{t+1}\mathbf{x}_{t+1}^H\boldsymbol{\Sigma}_t}{\mathbf{x}_{t+1}^H\boldsymbol{\Sigma}_t\mathbf{x}_{t+1}+\sigma^2}$
end for

Output: Designed combiners $\{\mathbf{w}_q\}_{q=1}^Q$, phase-shift vectors $\{\boldsymbol{\theta}_q\}_{q=1}^Q$, and observation matrix $\mathbf{X}$.

To achieve alternating optimization, we first reformulate the original problem (10) as the following two subproblems:

1) Fix $\boldsymbol{\theta}_{t+1}$ and Optimize $\mathbf{w}_{t+1}$: While fixing the phase-shift vector $\boldsymbol{\theta}_{t+1}$ and removing the unrelated parts, the original subproblem (10) can be reformulated as

$$\begin{aligned} \max_{\mathbf{w}_{t+1}} \quad & \mathbf{w}_{t+1}^H\left(\mathbf{I}_M \otimes \boldsymbol{\theta}_{t+1}^T\right)\boldsymbol{\Sigma}_t\left(\mathbf{I}_M \otimes \boldsymbol{\theta}_{t+1}^*\right)\mathbf{w}_{t+1} \\ \text{s.t.} \quad & |\mathbf{w}_{t+1}| = \frac{1}{\sqrt{M}}\mathbf{1}_M, \end{aligned} \tag{12}$$

where the reformulation is achieved by utilizing equality $\mathbf{w}_{t+1} \otimes \boldsymbol{\theta}_{t+1}^* = \left(\mathbf{I}_M \otimes \boldsymbol{\theta}_{t+1}^*\right)\mathbf{w}_{t+1}$.

2) Fix $\mathbf{w}_{t+1}$ and Optimize $\boldsymbol{\theta}_{t+1}$: Define the $\boldsymbol{\Sigma}_{t,m,m'} \in \mathbb{C}^{N\times N}$ as the (m,m')-th block of $\boldsymbol{\Sigma}_t$. Then, the posterior kernel can be rewritten as

$$\boldsymbol{\Sigma}_t = \begin{bmatrix} \boldsymbol{\Sigma}_{t,1,1} & \cdots & \boldsymbol{\Sigma}_{t,1,M} \\ \vdots & \ddots & \vdots \\ \boldsymbol{\Sigma}_{t,M,1} & \cdots & \boldsymbol{\Sigma}_{t,M,M} \end{bmatrix}. \tag{13}$$

By fixing $\mathbf{w}_{t+1}$ and removing the irrelevant components,

subproblem (10) can be rewritten as

$$\begin{aligned} \max_{\boldsymbol{\theta}_{t+1}} \quad & \boldsymbol{\theta}_{t+1}^H \left(\sum_{m=1}^{M} \sum_{m'=1}^{M} w_{t+1,m} w_{t+1,m'}^* \boldsymbol{\Sigma}_{t,m,m'}^* \right) \boldsymbol{\theta}_{t+1} \\ \text{s.t.} \quad & |\boldsymbol{\theta}_{t+1}| = \mathbf{1}_N, \end{aligned} \tag{14}$$

where $w_{t+1,m}$ is the m-th entry of $\mathbf{w}_{t+1}$.

Observing (12) and (14), one note that these subproblems share the same form of modules-constant quadratic programming. Thus, these two subproblems can be generalized as:

$$\begin{aligned} \max_{\mathbf{v}} \quad & \mathbf{v}^H \mathbf{U} \mathbf{v} \\ \text{s.t.} \quad & |\mathbf{v}| = \rho \mathbf{1}_K, \end{aligned} \tag{15}$$

where $\mathbf{v}$, $\mathbf{U}$, ρ, and K can be set to the corresponding variables in (12) and (14), respectively. Given the spherical geometric structure of the constraint set, i.e., $\mathcal{S} := \{\mathbf{v} \in \mathbb{C}^K : |\mathbf{v}| = \rho \mathbf{1}_K\}$, Riemannian manifold optimization perfectly matches to solve problem (15). Specifically, utilizing the relation $\mathbf{v}^H \mathbf{v} = K\rho^2$, the objective function in (15) can be equivalently replaced by

$$f(\mathbf{v}) = \mathbf{v}^H (\mathbf{U} + \alpha \mathbf{I}_K) \mathbf{v}, \tag{16}$$

where $\alpha > 0$ is a positive constant to ensure the algorithmic convergence. Given $f(\mathbf{v})$, the Euclidean gradient and the Riemannian gradient over the tangent space of $\mathcal{S}$ can be respectively written as:

$$\nabla f(\mathbf{v}) = (\mathbf{U} + \alpha \mathbf{I}_K) \mathbf{v}, \tag{17}$$

$$\mathbf{d}_{\mathcal{S}}(\mathbf{v}) = \nabla f(\mathbf{v}) - \frac{\mathbf{v} \odot \Re\left(\mathbf{v}^* \odot \nabla f(\mathbf{v})\right)}{\rho^2}. \tag{18}$$

In each iteration, the update over the tangent space can be written as

$$\mathbf{v} \leftarrow \rho \exp\left(j \angle \left(\mathbf{v} + \beta \mathbf{d}_{\mathcal{S}}(\mathbf{v})\right)\right) \tag{19}$$

where the retraction operation has been included to satisfy the constraint $\mathcal{S}$ and β is a constant step length. To ensure monotonic updates, the selection of α and β should satisfy the following principle [20]:

$$\alpha \geq \frac{K}{8} \lambda_{\max}(\mathbf{U}), \quad 0 < \beta < \frac{1}{\lambda_{\max}(\mathbf{U}) + \alpha}, \tag{20}$$

where $\lambda_{\max}(\cdot)$ denotes the largest eigenvalue of its argument. By respectively setting $\mathbf{v}$, $\mathbf{U}$, ρ, and K to the corresponding variables in (12) and (14), $\mathbf{w}_{t+1}$ and $\boldsymbol{\theta}_{t+1}$ can be alternatingly optimized until the convergence of ΔI_{t+1}. Consequently, we obtain the whole process of ARMO scheme in **Algorithm 1**.

Thanks to the Riemannian manifold optimization. With the step size in (20), the objective function is guaranteed to be non-decreasing in each iteration. Since the objective function is bounded due to the finite power constraint and the feasible set forms a compact manifold, the iterative procedure is guaranteed to converge to a stationary point. It is worth noting that, due to the non-convex nature of problem (8), the proposed greedy strategy does not guarantee global optimality. Fortunately, the sequential maximization of MI increment in (9) shares similarities with submodular optimizations, where greedy methods are known to achieve near-optimal performance under diminishing returns properties [21].

As the computational complexity of ARMO mainly depends on gradient computation, the overall complexity of **Algorithm 1** is $\mathcal{O}(QI_o(I_w M^2 + I_\theta N^2))$, where I_w, I_θ, and I_o are the required number of iterations for the convergence of $\mathbf{w}_{t+1}$, $\boldsymbol{\theta}_{t+1}$, and ΔI_{t+1}, respectively. This complexity is of the same order of magnitude as that of most RIS precoding algorithms[1]. In practical RIS-aided systems, the channel dimension MN may be very large. However, the kernel typically exhibits strong structure and can often be approximated as low-rank. This property can be exploited to reduce dimensionality. Moreover, the proposed observation matrix design is performed in a sequential manner, which avoids high-dimensional joint optimization. In addition, the kernel training and ARMO updates operate on a slower timescale, as the channel statistics vary much more slowly than instantaneous channels. These properties make the proposed method scalable in practice.

B. Acquisition of Channel Kernel

The implementation of ARMO scheme requires the knowledge of the kernel $\boldsymbol{\Sigma}_{\mathbf{h}}$. In real-world 5G New Radio systems, to enable minimum mean squared error (MMSE) channel estimation, $\boldsymbol{\Sigma}_{\mathbf{h}}$ is usually acquired via channel state information reference signals (CSI-RSs) [18], [19]. To extend this process to RIS-aided systems, we introduce an adaptive kernel training strategy, which smoothly integrates kernel learning into channel estimations without additional resources.

As a second-order statistic, the channel covariance $\boldsymbol{\Sigma}_{\mathbf{h}}$ varies much more slowly than the instantaneous channel $\mathbf{h}$. Consider a sliding window consisting of consecutive R frames, where the inter-frame channels $\mathbf{h}_r$ for all $r \in \{1, \cdots, R\}$ satisfy distribution $\mathcal{CN}(\mathbf{0}, \boldsymbol{\Sigma}_{\mathbf{h}})$. Our strategy is iteratively estimating the channels $\mathbf{h}_r$ and updating the sample kernel $\hat{\boldsymbol{\Sigma}}_{\mathbf{h}}$, such that the accuracy of estimator $\hat{\mathbf{h}}_r$ can be improved and $\hat{\boldsymbol{\Sigma}}_{\mathbf{h}}$ converges to the real kernel $\boldsymbol{\Sigma}_{\mathbf{h}}$ gradually. Let $\hat{\boldsymbol{\Sigma}}_{\mathbf{h}}^{(r)}$ denote the sample kernel in the r-th frame. Such a working flow process can be described as:

$$\begin{aligned} \hat{\boldsymbol{\Sigma}}_{\mathbf{h}}^{(0)} \underbrace{\overset{\text{ARMO}}{\rightarrow} \hat{\mathbf{h}}_1 \overset{(22)}{\rightarrow} \hat{\boldsymbol{\Sigma}}_{\mathbf{h}}^{(1)}}_{\text{frame 1}} \underbrace{\overset{\text{ARMO}}{\rightarrow} \hat{\mathbf{h}}_2 \overset{(22)}{\rightarrow} \hat{\boldsymbol{\Sigma}}_{\mathbf{h}}^{(2)}}_{\text{frame 2}} \overset{\text{ARMO}}{\rightarrow} \\ \cdots \underbrace{\overset{\text{ARMO}}{\rightarrow} \hat{\mathbf{h}}_R \overset{(22)}{\rightarrow} \hat{\boldsymbol{\Sigma}}_{\mathbf{h}}^{(R)}}_{\text{frame } R} \overset{\text{ARMO}}{\rightarrow} \cdots, \end{aligned} \tag{21}$$

where the sample kernel $\hat{\boldsymbol{\Sigma}}_{\mathbf{h}}^{(r)}$ is updated according to the estimated channel $\hat{\mathbf{h}}_r$. The following R-length sliding window is utilized to update the sample kernel in real time:

$$\hat{\boldsymbol{\Sigma}}_{\mathbf{h}}^{(r)} = \begin{cases} \frac{r-1}{r} \hat{\boldsymbol{\Sigma}}_{\mathbf{h}}^{(r-1)} + \frac{1}{r} \hat{\mathbf{h}}_r \hat{\mathbf{h}}_r^H, & \text{if } r \leq R, \\ \frac{1}{R} \sum_{r'=r-R}^{r} \hat{\mathbf{h}}_{r'} \hat{\mathbf{h}}_{r'}^H, & \text{if } r > R, \end{cases} \tag{22}$$

where the case when $r > R$ aims to track the time-varying $\boldsymbol{\Sigma}_{\mathbf{h}}^{(r)}$ in future frames. The sliding window size R introduces a trade-off between estimation accuracy and adaptability. A larger R improves the reliability of the covariance estimation

[1]Through simulations, we note that both the inner Riemannian optimization loops and the outer alternating updates in **Algorithm 1** converge rapidly with typical values $I_o = 3$ and $I_w = I_\theta = 15$.

by averaging over more samples, whereas a smaller R enhances the ability to track time-varying channel statistics.

To trigger the working flow in (21), an initial estimate of the channel covariance matrix is required. In practical systems, such an initial kernel can be obtained using existing kernel acquisition approaches such as [12]. Based on this initialization, the proposed adaptive kernel training scheme serves as a refinement mechanism to progressively improve the covariance estimation over time.

The proposed adaptive kernel learning strategy offers two main advantages. First, by initializing kernels as identity matrices, the method eliminates the need for prior knowledge of the actual kernels, rendering it suitable for a wide range of practical communication systems. Second, it enables simultaneous channel estimation and kernel training within a single frame by utilizing channels estimated by the ARMO algorithm for kernel training. This integration removes the need for a separate time period dedicated to kernel learning, significantly simplifying the frame structure and protocol in practice.

IV. Simulation Results

In this section, simulation results are carried out to verify the effectiveness of the proposed ARMO scheme.

A. Simulation Setup and Baselines

We consider the uplink channel estimation of an RIS-aided DAS. Without loss of generality, the uniform linear array (ULA) is equipped on the BS and the RIS is a uniform planar array (UPA). The dipole antennas are considered for the BS and the user, and patch antennas are deployed at the RIS. The electromagnetic mutual coupling effects among antennas/elements are calculated using Matlab Antenna Toolbox [22], and the clustered delay line (CDL)-A channel model defined in 3GPP TR 38.901 is adopted for simulations [23]. Otherwise specifically specified, the number of BS antennas and that of RIS elements are set as $M = 4$ and $N = 8 \times 8$, respectively. The antenna/element spacing is set to be $\lambda/4$. The signal-to-noise ratio (SNR) is defined as $\text{SNR} = 1/\sigma^2$, whose default value is set to 10 dB. The evaluation criterion of estimation accuracy is the normalized mean square error (NMSE), which is expressed as $\text{NMSE} = \mathsf{E}(\|\mathbf{h} - \hat{\mathbf{h}}\|^2/\|\mathbf{h}\|^2)$. The default value of pilot length is set to $Q = 200$.

To verify the effectiveness of the proposed ARMO based channel estimator, the following schemes are compared:

- **LS**: The classical least-square (LS) scheme is used for RIS channel estimation, i.e., $\hat{\mathbf{h}}_{\text{LS}} = (\mathbf{X}_{\text{LS}}^H)^\dagger \mathbf{y}_{\text{LS}}$. The BS combiner and the RIS phase-shift matrix in the observation matrix $\mathbf{X}_{\text{LS}}$ are generated from DFT vectors.
- **MMSE**: Assume the kernel $\mathbf{\Sigma_h}$ is perfectly known. Using the same setting as the LS estimator, the MMSE estimator in [13] is adopted to recover RIS channel $\mathbf{h}$ via (6).
- **OMP**: The orthogonal matching pursuit (OMP) method proposed in [11] is used to recover RIS channel $\mathbf{h}$. To satisfy the restricted isometry property, the BS combiner and the RIS phase-shift matrix are randomly generated.
- **Ice filling**: Assume the kernel $\mathbf{\Sigma_h}$ is perfectly known and the RIS phase-shift matrix is randomly generated. The ice filling scheme in [16] is used to design the BS combiner. Then, $\mathbf{h}$ is estimated via the MMSE estimator (6).
- **ARMO (Ideal kernel)**: Assume $\mathbf{\Sigma_h}$ is perfectly known. The proposed ARMO scheme in **Algorithm 1** is employed to jointly design $\mathbf{X}$. Based on $\mathbf{X}$ and $\mathbf{\Sigma_h}$, the MMSE estimator in (6) is employed to recover $\mathbf{h}$.
- **ARMO (Kernel training)**: The working flow process in (21) and (22) is employed to acquire and update the kernel $\hat{\mathbf{\Sigma}}_{\mathbf{h}}$. For kernel tracking, the length of the sliding window is set to $R = 100$. The initial kernel $\hat{\mathbf{\Sigma}}_{\mathbf{h}}^{(0)}$ is generated using the sample covariance of R independently estimated channels, which are obtained via LS estimation. Then, $\hat{\mathbf{\Sigma}}_{\mathbf{h}}$ is used as the input of **Algorithm 1**. Based on the designed $\hat{\mathbf{X}}$ and $\hat{\mathbf{\Sigma}}_{\mathbf{h}}$, the MMSE estimator in (6) is employed to recover $\mathbf{h}$.

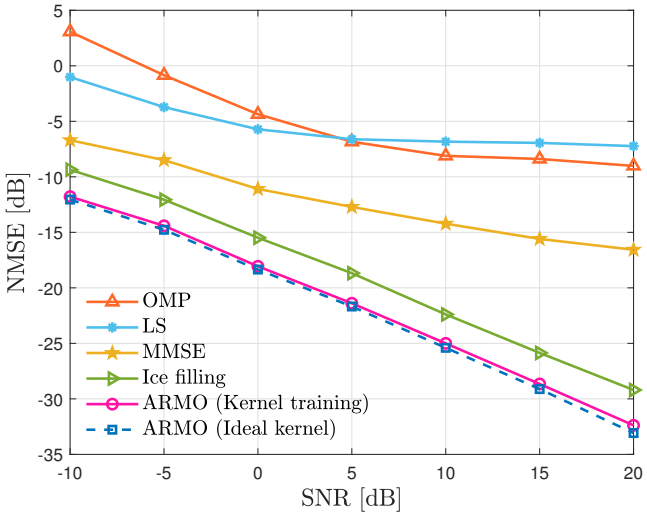

Fig. 1. NMSE performance versus SNR for different schemes.

B. Estimation Accuracy versus SNR

Firstly, we plot the NMSE as a function of SNR in Fig. 1. It can be observed that, compared with the estimators without utilizing the prior information of kernels (LS and OMP), the schemes utilizing kernels (MMSE, ice filling, and ARMO) demonstrate their advantage in estimation accuracy. For example, thanks to the carefully designed combiners at the BS, the ice filling scheme outperforms the MMSE scheme whose BS combiners are generated from the DFT matrix. Furthermore, since our proposed ARMO schemes jointly design the BS combiners and the phase-shift matrix at the RIS, they can achieve higher performance gains than the ice filling scheme that only focuses on the BS combiner design. Besides, it is worth noting that, the ARMO scheme with kernel training achieves a very similar performance to that with perfect kernel knowledge. It indicates that, by alternatingly updating the kernel and channels, the knowledge of the real kernel is no longer necessary for the implementation of ARMO in practice.

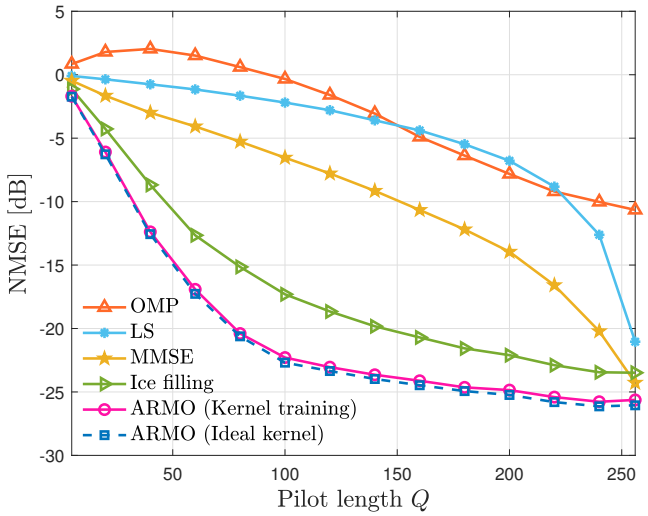

Fig. 2. NMSE performance versus pilot length Q for different schemes.

C. Estimation Accuracy versus Pilot Length

Then, we plot the NMSE as a function of pilot length Q in Fig. 2. One can find that, with the assistance of the kernel, the kernel-related schemes can achieve considerable performance with a small number of pilots. In particular, the proposed ARMO schemes have an obvious superiority in estimation accuracy. For example, to achieve an NMSE of -10 dB, the required pilot lengths Q for OMP, LS, MMSE, ice filling, ARMO (kernel training), and ARMO (ideal kernel) are 240, 225, 150, 45, 30, and 30, respectively. Note that, the OMP estimator does not perform well. It is because the small antenna spacing leads to the spatial oversampling and mutual coupling among antennas, thus the channels of DASs no longer enjoy the angular-domain sparse property. Furthermore, when the pilot length is sufficiently large (e.g., $Q = 256$), the kernel-related schemes converge to a similar estimation accuracy. This occurs because the observation matrix of the MMSE estimator becomes a complete DFT matrix, which can fully characterize all channel patterns of DASs. Under these conditions, the accuracy gain from a carefully designed observation matrix becomes marginal. It is worth noting that, the number of RIS elements can be very large in practice, making it impractical to allocate a large number of pilots due to limited signaling overhead. Therefore, the most practically relevant regime for the considered RIS-aided systems corresponds to the case when $Q \ll MN$.

V. Conclusions

This paper proposed an observation matrix design framework to enhance channel estimation in RIS-aided DASs. By formulating the design as an MI maximization problem within a Bayesian framework, we jointly optimized the receiver combiners and RIS phase-shift matrices using ARMO scheme. In addition, an adaptive kernel learning strategy was introduced to enable simultaneous channel estimation and kernel training. Simulation results verified that the proposed method achieves noticeable performance gains over existing schemes, particularly in the low-pilot regime.

References

[1] C. Huang, S. Hu, G. C. Alexandropoulos, A. Zappone, C. Yuen, R. Zhang, M. D. Renzo, and M. Debbah, "Holographic MIMO surfaces for 6G wireless networks: Opportunities, challenges, and trends," *IEEE Wireless Commun.*, vol. 27, no. 5, pp. 118–125, Oct. 2020.

[2] Z. Zhang and L. Dai, "Pattern-division multiplexing for multi-user continuous-aperture MIMO," *IEEE J. Sel. Areas Commun.*, vol. 41, no. 8, pp. 2350–2366, Aug. 2023.

[3] I. Kanbaz, O. Yurduseven, and M. Matthaiou, "Super-directive antenna arrays: How many elements do we need?" *arXiv preprint arXiv:2401.09179*, Jan. 2024.

[4] K.-K. Wong and K.-F. Tong, "Fluid antenna multiple access," *IEEE Trans. Wireless Commun.*, vol. 21, no. 7, pp. 4801–4815, Jul. 2021.

[5] Q. Li, M. El-Hajjar, C. Xu, J. An, C. Yuen, and L. Hanzo, "Stacked intelligent metasurfaces for holographic MIMO-aided cell-free networks," *IEEE Trans. Commun.*, vol. 72, no. 11, pp. 7139–7151, Nov. 2024.

[6] Q. Li, M. El-Hajjar, K. Cao, C. Xu, H. Haas, and L. Hanzo, "Holographic metasurface-based beamforming for multi-altitude LEO satellite networks," *IEEE Trans. Wireless Commun.*, vol. 24, no. 4, pp. 3103–3116, Apr. 2025.

[7] Q. Li, M. El-Hajjar, Y. Sun, and L. Hanzo, "Performance analysis of reconfigurable holographic surfaces in the near-field scenario of cell-free networks under hardware impairments," *IEEE Trans. Wireless Commun.*, vol. 23, no. 9, pp. 11 972–11 984, Sep. 2024.

[8] Z. Zhang and L. Dai, "Reconfigurable intelligent surfaces for 6G: Nine fundamental issues and one critical problem," *Tsinghua Sci. Technol.*, vol. 28, no. 5, pp. 929–939, Oct. 2023.

[9] P. Wang, J. Fang, H. Duan, and H. Li, "Compressed channel estimation for intelligent reflecting surface-assisted millimeter wave systems," *IEEE Signal Process. Lett.*, vol. 27, pp. 905–909, May 2020.

[10] C. Hu, L. Dai, S. Han, and X. Wang, "Two-timescale channel estimation for reconfigurable intelligent surface aided wireless communications," *IEEE Trans. Commun.*, vol. 69, no. 11, pp. 7736–7747, Nov. 2021.

[11] X. Wei, D. Shen, and L. Dai, "Channel estimation for RIS assisted wireless communications—part II: An improved solution based on double-structured sparsity," *IEEE Commun. Lett.*, vol. 25, no. 5, pp. 1403–1407, May 2021.

[12] M. Qian, C. Li, Y. Ma, Y. Song, C. Liu, and Z. Yin, "A contextual MAB-based two-timescale scheme for RIS-assisted systems," *IEEE Wireless Commun. Lett.*, vol. 14, no. 2, pp. 400–404, Feb. 2024.

[13] Q.-U.-A. Nadeem, H. Alwazani, A. Kammoun, A. Chaaban, M. Debbah, and M.-S. Alouini, "Intelligent reflecting surface-assisted multi-user MISO communication: Channel estimation and beamforming design," *IEEE Open J. Commun. Society*, vol. 1, pp. 661–680, May 2020.

[14] A. Pizzo and A. Lozano, "Mutual coupling in holographic MIMO: Physical modeling and information-theoretic analysis," *IEEE J. Sel. Areas Inf. Theory*, vol. 6, pp. 111–126, May 2025.

[15] N. Kolomvakis and E. Björnson, "Exploiting mutual coupling characteristics for channel estimation in holographic MIMO," in *Proc. IEEE Global Commun. Conf. (IEEE GLOBECOM'24)*, 2024, pp. 3570–3575.

[16] M. Cui, Z. Zhang, L. Dai, and K. Huang, "Ice-filling: Near-optimal channel estimation for dense array systems," *IEEE Trans. Wireless Commun.*, vol. 24, no. 10, pp. 8551–8564, Oct. 2025.

[17] Z. Zhang, J. Zhu, L. Dai, and R. W. Heath, "Successive Bayesian reconstructor for channel estimation in fluid antenna systems," *IEEE Trans. Wireless Commun.*, vol. 24, no. 3, pp. 1992–2006, Mar. 2025.

[18] S. Park and R. W. Heath, "Spatial channel covariance estimation for the hybrid MIMO architecture: A compressive sensing-based approach," *IEEE Trans. Wireless Commun.*, vol. 17, no. 12, pp. 8047–8062, Dec. 2018.

[19] K. Upadhya and S. A. Vorobyov, "Covariance matrix estimation for massive MIMO," *IEEE Signal Process. Lett.*, vol. 25, no. 4, pp. 546–550, Apr. 2018.

[20] K. Alhujaili, V. Monga, and M. Rangaswamy, "Transmit MIMO radar beampattern design via optimization on the complex circle manifold," *IEEE Trans. Signal Process.*, vol. 67, no. 13, pp. 3561–3575, 2019.

[21] G. L. Nemhauser, L. A. Wolsey, and M. L. Fisher, "An analysis of approximations for maximizing submodular set functions—i," *Mathematical programming*, vol. 14, no. 1, pp. 265–294, 1978.

[22] MathWorks, "Antenna toolbox," Natick, MA, 2024. [Online]. Available: https://www.mathworks.com/products/antenna.html

[23] 3GPP TR, "Study on channel model for frequencies from 0.5 to 100 GHz," *3GPP TR 38.901 version 14.0.0 Release*, Dec. 2019.